Society for Science and Education
United Kingdom

ISSN: 2055 - 1266
Volume 3 No 2
April 2016

Journal of Biomedical Engineering and Medical Imaging

TABLE OF CONTENTS

EDITORIAL ADVISORY BOARD

Professor Kenji Suzuki
Department of Radiology, University of Chicago
United States

Professor Habib Zaidi
Dept. of Radiology, Div. of Nuclear Medicine, Geneva University Hospital, Geneva, Swaziland

Professor Tzung-Pe
National University of Kaohsiung,, Taiwan
China

Professor Nicoladie Tam
Dept. of Biological Sciences, University of North Texas, Denton, Texas, United States

Professor David J Yang
The University of Texas MD Anderson Cancer Center, Houston
United States

Professor Ge Wang
Biomedical Imaging Center, Rensselaer Polytechnic Institute. Troy, New York
United States

Dr Hafiz M. R. Khan
Department of Biostatistics, Florida International University
United States

Dr Saad Zakko
Director of Nuclear Medicne Dubai Hospital
UAE

Dr Abdul Basit
Malaysia School of Information Technology, Monash University
Malaysia

DISCLAIMER

All the contributions are published in good faith and intentions to promote and encourage research activities around the globe. The contributions are property of their respective authors/owners and the journal is not responsible for any content that hurts someone's views or feelings etc.

SOCIETY FOR SCIENCE AND EDUCATION UNITED KINGDOM

JBEMi JOURNAL OF BIOMEDICAL ENGINEERING AND MEDICAL IMAGING

ISSN: 2055-1266
VOLUME 3 ISSUE 2

Segmentation of Salivary Glands in Nuclear medicine Images Using Edge Detection Tools

Yousif Mohamed Y. Abdallah
Department of Radiological Sciences and medical Imaging, College of Medical Applied Sciences, Majmaah University
y.yousif@mu.edu.sa

ABSTRACT

Recognition of the Salivary glands in nuclear medicine examination is very difficult because of unclear borders and existence of noise, which affects the spatial resolution and reduces the diagnostic values of those images Therefore, image-processing programs such as MatLab, has powerful tools, which can use for solving those problems. The Morphology tool frequently applied to this problem. In this paper, I used *entropyfilt* function to create a texture image. This function returns an array where each output pixel contains the entropy value of the 9-by-9 neighborhood around the corresponding pixel in the salivary glands scintigraphy images. Threshold the rescaled image to segment the textures. A threshold value of 0.8 selected because it was roughly the intensity value of pixels along the boundary between the textures. The segmented images compare the binary image *rough Mask* to the original image. The quantitative results calculated using a measure of percentage match between ground truth and segmentation results. The percentage match (PM) measure was 99.33 (p <0.05) and Corresponding Ratio (CR) was -0.007 p <0.05). The proposed method is able to recognize the salivary glands accurately.

Keywords; Salivary glands; MatLab; Scintigraphy; Morphology.

1 Introduction

Image segmentation has been a long-standing problem in computer vision. It is a very difficult problem for general images, which may contain effects such as highlights, shadows, transparency, and object occlusion. Segmentation in the domain of medical imaging has some characteristics that make the segmentation task easier and difficult at the same time [1]. On the one hand, the imaging is narrowly focused on an anatomic region. The imaging context is also well defined. While context may be present to some extent in segmenting general images (e.g., indoor vs. outdoor, city vs. nature, people vs. animals), it is much more precise in a medical imaging task, where the imaging modality, imaging conditions, and the organ identity is known [2]. In addition, the pose variations are limited, and there is usually prior knowledge of the number of tissues and the Region of Interest (ROI) [3] [4]. On the other hand, the images produced in this field are one of the most challenging due to the poor quality of imaging making the anatomical region segmentation from the background very difficult. Often the intensity variations alone are not sufficient to distinguish the foreground from the background, and

DOI: 10.14738/jbemi.32.1702
Publication Date: 15th March 2016
URL: http://dx.doi.org/10.14738/jbemi. 32.1702

additional cues are required to isolate ROIs [5]. Finally, segmentation is often a means to an end in medical imaging. It could be part of a detection process such as tissue detection, or for the purpose of quantification of measures important for diagnosis, such as for example, lesion burden which is the number of pixels/voxels within the lesion regions in the brain [6]. In general, the information contained in an image modeled in several ways. A simple approach is to record the intensity distribution within an image via a One-dimensional (1D) histogram and use simple thresholding to obtain the various segments. Several variations on classical histogram thresholding proposed for medical image segmentation that incorporate extended image representation schemes as well as advanced information modeling [7]. Multi-dimensional histograms formed from the intensity values produced by each of the imaging protocols. It is often the case that several acquisitions are available for the same image. Spatial information: Since intensity histograms do not preserve spatial contiguity of pixels, one variation is to add spatial position (x, y) or (x, y, z) to form a multi-dimensional feature vector incorporating spatial layout. If the medical images are in a time sequence (e.g. moving medical imagery), then time can be added as an additional feature in the representation space [8] [9]. Thus, these approaches represent each image pixel as a feature vector in a defined multi-dimensional feature space. The segmentation task can be seen as a combination of two main processes; modeling which is the generation of a representation over a selected feature space [11]. This can be termed the modeling stage. The model components viewed as groups, or clusters in the high-dimensional space [12]. In order to be directly relevant for a segmentation task, the clusters in the model should represent homogeneous regions of the image. In general, the better the image modeling, the better the segmentation produced. Since the number of clusters in the feature space are often unknown, segmentation regarded as an unsupervised clustering task in the high dimensional feature space [13].

1.1 Materials and Methods

This was experimental study conducted to recognize the salivary glands scintigraphy images using image-processing program using basic morphology tools. For salivary glands scintography images treated by using image processing program (MatLab), where the recognition was studied. The scanned image saved in a PNG file format to preserve the quality of the image. Salivary glands could easily detect in nuclear medicine images if the object had sufficient contrast from the background. The Steps of recognition were as shown in figure 1.

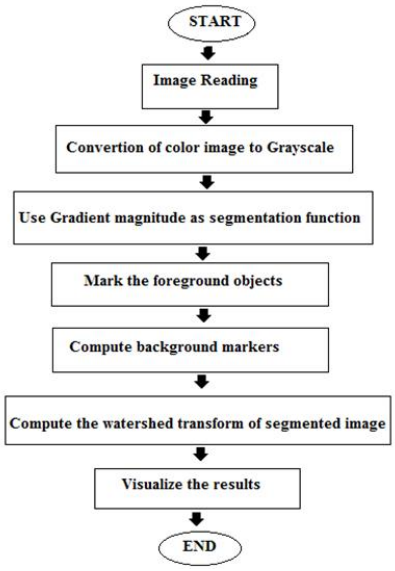

Figure 1. Steps of liver segmentation using MatLab program

2 The results

This was experimental study conducted to recognize the salivary glands scintigraphy images using image-processing program using basic morphology tools. The segmentation of image started firstly by reading image as shown in (Figure 1).

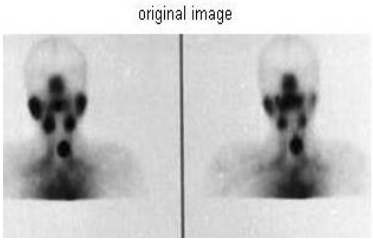

Figure 2. Original image used for Segmentation

The salivary glands are present in this image and they can be seen in them entirety. I detected or segmented those glands. The object segmented differs greatly in contrast from the background image. Operators that calculate the gradient of an image in contrast could detect changes. The gradient image could calculate and a threshold could apply to create a binary mask containing the segmented cell. First, I use edge and the Sobel operator to calculate the threshold value. I then tune the threshold value and use edge again to obtain a binary mask that contains the segmented salivary glands as shown in (Figure 2).

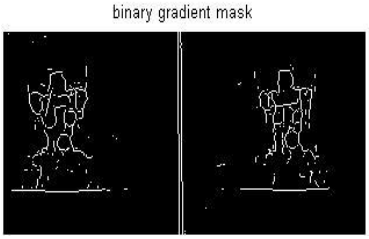

Figure 2. Binary Gradient Magnitude Mask

The binary gradient mask shows lines of high contrast in the image. These lines do not quite delineate the outline of the object of interest. Compared to the original image, I can see gaps in the lines surrounding the object in the gradient mask. These linear gaps will disappear if the Sobel image is dilated using linear structuring elements, which we can create with the strel function. The binary gradient mask dilated using the vertical structuring element followed by the horizontal structuring element. The imdilate function dilates the image as shown in figure 3.

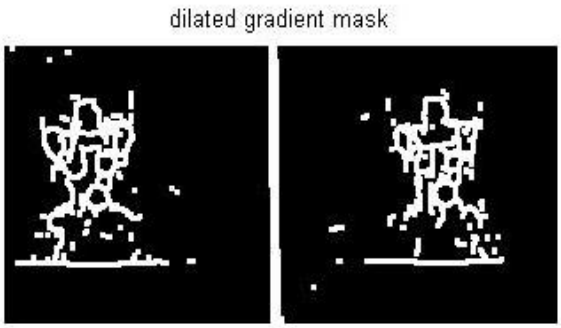

Figure 3. The dilated gradient mask

The dilated gradient mask shows the outline of the thyroid quite nicely, but there are still holes in the interior of the lungs. To fill these holes we use the imfill function as shown in figure 4.

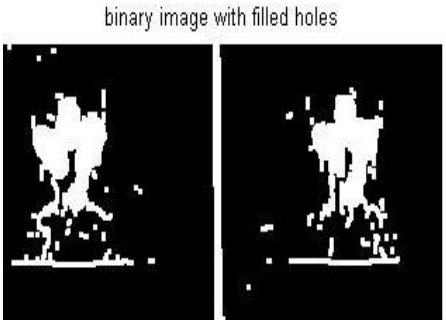

Figure 4. Binary image with filled holes

The salivary gland have been successfully segmented, but it is not the only object that has been found. Any objects that connected to the border of the image can be removed using the imclearborder function. The connectivity in the imclearborder function was set to 4 to remove diagonal connections as shown in figure 5.

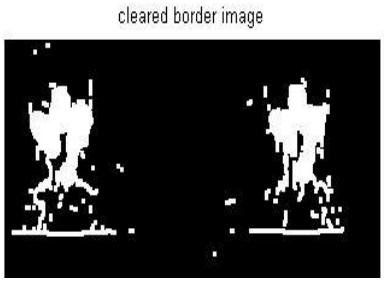

Figure 5. Cleared Border image

Finally, in order to make the segmented object look natural, we smoothen the object by eroding the image twice with a diamond structuring element. I create the diamond structuring element using the strel function as shown in figure 6.

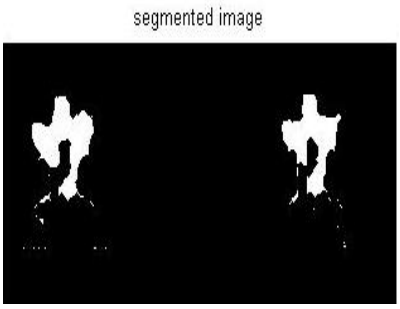

Figure 6. The segmented image

An alternate method for displaying the segmented object would be to place an outline around the segmented thyroid. The outline created by the bwperim function figure 7.

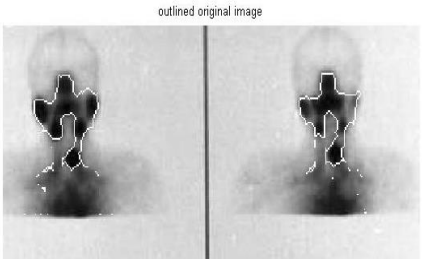

Figure 7. The Outlined original image

3 Conclusion

The smoothing of the object by eroding the image twice with a diamond-structuring element using the strel function will create the diamond-structuring element, which is useful of natural look of segmented object. So conclusion of this paper that edge detection and basic morphology tools are best tools to detect salivary glands. The detection of the noise is a complex procedure, which is difficult to detect by naked eye so that image analysis should perform by using powerful image processing. A watershed transform Algorithm lungs segmentation method proposed in this study. Proposed method is able to determine the salivary glands boundaries accurately. It is able to segment salivary glands and improves radiological analysis and diagnosis.

REFERENCES

[1] Abdallah, Y., Hayder, A., and Wagiallah ,E., *Automatic Enhancement of Mammogram using Contrast Algorithm*. International Journal of Science and Research (IJSR), 2014. 3(9): p. 1886-1891.

[2] Abdelwahab, R., and Abdallah, Y., Hayder, A., and Wagiallah ,E., Application of Texture Analysis *Algorithm for Data Extraction in Dental X-Ray Images*. International Journal of Science and Research (IJSR), 2014. 3(10): p. 1934-1939.

[3] Abdallah, Y., Alkhir, M., Algaddal, A., *Improvement of Brain Tumors Detection Using Markers and Boundaries Transform*. International Journal of Science and Research (IJSR), 2015. 4(1): p. 2372-2378.

[4] Bidgood, D. & Horii, S., Introduction to the ACR-NEMA DICOM standard. RadioGraphics, 1992. 12: p. 345-355.

[5] Lehmann, T.M.; Gönner, C. & Spitzer, K., Survey: Interpolation Methods in Medical Image Processing. IEEE Transactions on Medical Imagin: 1999. 18(11): p. 1049-1075

[6] Li, G. & Miller, R.W., Volumetric Image Registration of Multi-modality Images of CT, MRI and PET, Biomedical Imaging. Youxin Mao (Ed.), 2010.

[7] Abdallah, Y., Application of Analysis Approach in Noise Estimation, Using Image Processing Program. Lambert Publishing Press GmbH & Co. KG, Germany, 2011.

[8] Lyra, M.; Sotiropoulos, M., Lagopati, N. & Gavrilleli, M. , Quantification of Myocardial Perfusion in 3D SPECT images – Stress/Rest volume differences, Imaging Systems and Techniques (IST), IEEE International Conference 2010: p. 31 – 35

[9] Narasimha-Iyer, H., et al., *Automatic Identification of Retinal Arteries and Veins From Dual-Wavelength Images Using Structural and Functional Features.* Biomedical Engineering, IEEE Transactions, 2007. 54(8): p. 1427-1435.

[10] Abdallah, Y., and Wagiallah, E., *Segmentation of Thyroid Scintography Using Edge Detection and Morphology Filters*. International Journal of Science and Research (IJSR), 2014. 3(11): p. 2768-2772.

[11] Abdallah, Y., and Hassan, A., *Segmentation of Brain in MRI Images Using Watershed-based Technique*. International Journal of Science and Research (IJSR), 2015. 4(1): p. 683-688.

[12] Hong, S., et al., *Optimal scheduling of tracing computations for real-time vascular landmark extraction from retinal fundus images.* Information Technology in Biomedicine, IEEE Transactions on, 2001. 5(1): p. 77-91.

[13] Pinz, A., et al., *Mapping the human retina.* Medical Imaging, IEEE Transactions on, 1998. 17(4): p. 606-619.

[14] Abdallah, Y., and Yousef R., Augmentation of X-Rays Images using Pixel Intensity Values Adjustments. International Journal of Science and Research (IJSR), 2015. 4(2): p. 2425-2430.

[15] Meyer, Fernand, "Topographic distance and watershed lines," Signal Processing , Vol. 38, July 1994, pp. 113-125

SOCIETY FOR SCIENCE AND EDUCATION UNITED KINGDOM

JBEMi JOURNAL OF BIOMEDICAL ENGINEERING AND MEDICAL IMAGING

ISSN: 2055-1266
VOLUME 3 ISSUE 2

MRI Segmentation based on Multiobjective Fuzzy Clustering

Olfa Mohamed Limam
Institut Supérieur d'Informatique, University Tunis EL Manar, Tunis, Tunisie
limemolfa@yahoo.fr

ABSTRACT

Brain image segmentation has a major role in medical image analysis for better interpretation of complex medical diagnosis such as tumor detection. The challenge of brain tumor detection is to detect accurately the tumor portion inside the brain image. In this work, we propose a multiobjective clustering framework to separate tumor regions from a brain image based on the neighbor nearest strategy. Applied to magnetic resonance image brain, our method provides an accurate identification of brain tumor.

Keywords: Brain tumor detection, fuzzy clustering, multiobjective optimization, neighbor nearest strategy.

1 Introduction

Brain tumor detection is a challenging task in medical image processing [1]. Brain tumor detection problem is termed as clustering problem while it consists in partitioning a given image into different regions [3]. Therefore, it is obvious to apply clustering for the distinction of tumor tissues from other healthy tissues for medical images [4].

Most conventional clustering methods assign each pixel to a one single region. While, boundaries between regions are not clearly defined [4]. So, fuzzy clustering is more appropriate to detect tumor in brain images [5]. Fuzzy clustering has been widely applied for brain image segmentation [6]. Li et al. [7], Pham and Prince [8] used FCM algorithm. Maksoud et al. [9] used K-means clustering technique combined with FCM algorithm. Udupa and Pnuam [10] used the fuzzy connectedness for abnormal tissue segmentation. However, these methods are very sensitive to noise. Hence, hybrid methods was applied in order to get desired results. Menon et al. [11] and Alsmadi [12] combined FCM with artificial bee colony algorithm. However, single fuzzy clustering is not recommended since single validity index fails to cope with different types of data sets. Moreover, the wrong choice of a single clustering measure may conduct to unsatisfying segmentation results [5]. Then, several multiobjective approaches have been proposed to segment brain images [13]. Acharya et al. [14] used simulated annealing for classification of cancer data sets. Three cluster validity indices are optimized namely XB, PBM, and FCM indices, to accurately reflect tissue clusters. Mukhopadhyay et al. [15] used NSGA-II to optimize the same three objective functions. Saha and Bandyopadhyay [16] proposed a genetic clustering technique and in [17] they proposed variable length genetic clustering technique to segment brain image data sets.

DOI: 10.14738/jbemi.32.1959
Publication Date: 12th April 2016
URL: http://dx.doi.org/10.14738/jbemi. 32.1959

However, most multiobjective fuzzy clustering techniques are developed for brain image segmentation and not for tumor detection and optimized with at most two objective functions. In previous work, Limam [18] proposed a multiobjective fuzzy genetic clustering technique optimizing two objective functions, the spatial compactness and the spatial separateness of clusters for brain tumor detection.

In this work, we propose a multiobjective fuzzy clustering method for brain tumor detection using three objective functions based on different data properties, namely, the fuzzy neighbor nearest connectedness, the fuzzy variance cluster and the external c cluster validity index Minkowski score. Our method generates an ensemble of Pareto solutions and we use the Minkowski score to select the final segmented image. Therefore, this paper develops a new multiobjective fuzzy clustering approach for brain tumor detection in MRI images to accurately diagnose the region of cancer. The main problem of works is that the quantitative results done by different works for their proposed methods are tested on different datasets rather than a common standard dataset. Also, the absence of a standard measure to compare classification accuracy of algorithms .

This paper is organized as follows. Section 2 details our proposed method. Section 3 illustrates the experimental study. Section 4 presents a conclusion.

2 The Multiobjective Fuzzy Clustering Method

The different steps of our proposed method are detailed in the following sections.

2.1 Color features

In order to improve the quality of the resulting segmentation, color features are used [19]. The standard RGB color space is used by our proposed algorithm.

2.2 Pattern proximity

The Euclidean distance is used to calculate the pattern proximity [20]. In general, the distance between two pixels x: $(x_1, ..., x_n)$ and y: $(y_1, ..., y_n)$ in an Euclidean n-space is given by

$$d(x,y) = |x - y| = \sqrt{\sum_{i=1}^{n} |x_i - y_i|^2} \quad (1)$$

2.3 Multiobjective fuzzy clustering algorithm

NSGA-II is adopted as the underlying multiobjective framework for fuzzy clustering. NSGA-II inputs arguments are the population size, an upper bound of the number of clusters, the data set, and a maximum number of generations. At the beginning of the algorithm, an initial potential solutions should be defined.

2.3.1 Initialization Step

In NSGA-II based clustering, chromosomes encodes the centers of the partitions. So, in the initial NSGA population, initial centers are encoded using FCM in order to provide more accurate solutions. FCM produces C cluster centers and a C x N membership matrix U(x).

2.3.2 Fitness Functions Computation

Three cluster validity measure are used to quantify the quality of each obtained chromosome. The fuzzy neighbor nearest connectedness index, fuzzy variance of clusters and Minkowski index, are simultaneously optimized and computed for each chromosome. To compute the objective functions, we extract the centers encoded in a given chromosome. The fuzzy neighbor nearest connectedness NN_c index, is defined by

$$NN_c = \sum_{i=1}^{C} \frac{\sigma_i}{n_i} = \sum_{i=1}^{C} \frac{\sum_{k=1}^{N} {f_{ik}}^m D(v_i, x_k)}{\sum_{k=1}^{N} {f_{ik}}^m} \tag{2}$$

where m the fuzzy exponent , $D(v_i, x_k)$ defines the Euclidean distance between i^{th} cluster center and k^{th} data point, σ_i denotes the variation of clusters and n_i the fuzzy cardinality of the i^{th} cluster is given by:

$$n_i = \sum_{k=1}^{N} {f_{ik}}^m, 1 \le i \le C. \tag{3}$$

The conditional membership function of a pixel f_{ik} is defined as

$$f_{ik} = \frac{u_{ik} h_{ik}}{\sum_{j=1}^{C} u_{jk} h_{jk}}, \tag{4}$$

where the membership degree u_{ik} is defined as

$$u_{ik} = \frac{1}{\sum_{j=1}^{C} \left(\frac{D(v_i, x_k)}{D(v_j, x_k)} \right)^{\frac{2}{m-1}}} \tag{5}$$

and h_{ik} , the level of pixel x_k belonging to the i^{th} cluster based on its neighborhood in a spatial domain, is defined as follows:

$$h_{ik} = \sum_{k \in Nb(x_k)} g_{ik}, \tag{6}$$

with

$$g_{ik} = \begin{Bmatrix} 1 & if \quad u_{ik} = \max\{u_{lk}\}, for \quad l = 1, ..., C \\ 0 & otherwise \end{Bmatrix} \tag{7}$$

where $NB(x_k)$ represents a square neighborhood having pixel x_k in its center. We used a pixel Window of 3x3. The fuzzy variance of clusters V is given by

$$V = \sum_{i=1}^{C} \sum_{i=1, j \neq i}^{C} f_{ij}^{\ m} \ D(v_i, v_j). \tag{8}$$

where $D(v_i, v_j)$ the Euclidean distance between clusters v_i and v_j .

The external cluster validity index Minkowksi score (MS), measuring the agreement between the true clustering T and the obtained clustering U, is given by:

$$MS(T,U) = \sqrt{\frac{n_{01} + n_{10}}{n_{11} + n_{10}}} \tag{9}$$

where n_{11} is the total number points assigned to the same clusters in both T and U, n_{01} the total number of pairs of points that are assigned only in the same cluster of U and n_{10} the total number of pairs of points that are assigned to the same cluster of T but in a different cluster of U. Hence, the fuzzy neighbor nearest connectedness measure NN_c should be minimized, the fuzzy variance V should be maximized and the Minkowski score MS should be minimized, as follows:

$$\begin{cases} \text{Min } NN_c \\ \text{Max } V \\ \text{Min MS} \end{cases}$$

2.3.3 Genetic Operators

Crowded binary tournament selection is adopted to generate the mating set of chromosomes, conventional crossover and mutation are utilized. The NSGA-II final step is its elitism operation, where the Pareto solutions among the parent and child populations are propagated to the next generation. The NSGA based clustering algorithm provides a set of solutions on the final Pareto optimal front.

2.4 Optimal solution

The final part of the multiobjective fuzzy clustering algorithm is chosen as the best solution from a set of solutions based on a validity measure MS index [21]. The best partition corresponds to the minimum value of MS index [21].

3 Experiments and Analysis

Segmentation results are analyzed based on a visual experimental study applied to three simulated brain tumor image data sets illustrating different tumor locations. The following Figures present different tumor types inside the brain stem. The simulated brain MR images can be downloaded from Brainweb [22].

The evolutionary parameters of our method are set as follows: the population size is 20, the number of generations is equal to 20, the crossover probability is 0.8 and mutation probability is set to be 0.01. The number of clusters used are between 2 and 16 and the fuzzy factor m is set to 2. The (a) parts of Figures

(1), (2) and (3) show the original MRI brain tumor images and the (b) parts show the segmented images generated by our method.

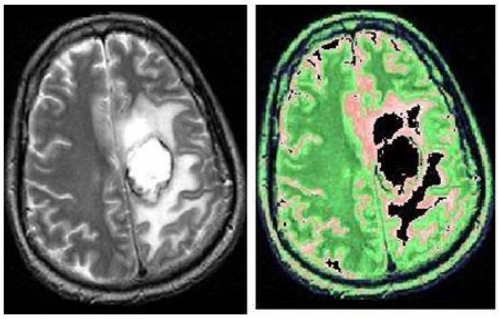

Figure 1 (a) Original MRI brain tumor image (b) Image segmented by our method

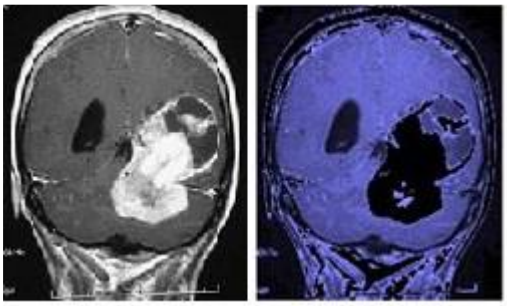

Figure 2 (a) Original MRI brain tumor image (b) Image segmented by our method

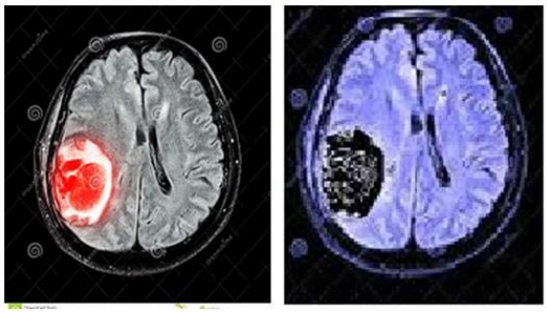

Figure 3 (a) Original MRI brain tumor image (b) Image segmented by our method

In previous Figures, our method succeeds to locate the tumor part of the brain and clearly separates it from the other parts of the brain. Results shows that for the different images, our method makes a clear identification of the tumor portion in the brain.

4 Conclusion

This paper presents a multiobjective fuzzy clustering method that optimizes three objectives. A visual comparison applied to MRI brain image was conducted in order to show the effectiveness of our proposed method to detect brain tumor images. Our proposed approach can be extended to detect other types of tumors in other medical imagery types.

REFERENCES

[1] Shen Shan, Sandham William, Granat Malcolm and Sterr Annette. Mri fuzzy segmentation of brain tissue using neighborhood attraction with neural-network optimization. IEEE Transactions on Information Technology in Biomedicine, 9(3):459–467, 2005.

[2] P.Tamije Selvy, V. Palanisamy, and T. Purusothaman. Performance analysis of clustering algorithms in brain tumor detection of mr images. European Journal of Scientific Research, 62(3):321–330, 2011.

[3] Suchita Yadav and Meshram Sachin. Brain tumor detection using clustering method. International Journal of Computational Engineering Research, 3(4):11–14, 2013.

[4] Miin-Shen Yang, Yu-Jen Hu, Karen Chia-Ren and Charles Chia-Lee Lin. Segmentation techniques for tissue differentiation in mri of ophthalmology using fuzzy clustering algorithms. Magentic resonance Imaging, 20:173–179, 2002.

[5] Sanghamitra Bandyopadhyay, Anirban Mukhopadyay, and Ujjwal. Maulik. Combining multiobjective fuzzy clustering and probabilistic ANN classifier for unsupervised pattern classification: Application to satellite image segmentation. IEEE on Evolutionary Computation, pages 877–883, 2008.

[6] Weibei Dou, Su Ruan, Daniel Bloyet, and Jean-Marc Constans. A framework of fuzzy information fusion for the segmentation of brain tumor tissues on mr images. Image and Vision Computing, 25(2):164–171, 2007.

[7] Chunlin Li, DB Goldgof, and LO Hall. Knowledge-based classification and tissue labeling of mr images of human brain. IEEE transactions on Medical Imaging, 12(4):740–750, 2002.

[8] L. Dzung Pham and Jerry L. Prince. Knowledge-based classification and tissue labeling of mr images of human brain. IEEE transactions on Medical Imaging, 18(9):737–752, 1999.

[9] Eman A. Abdel Maksoud, Mohammed Elmogy, and Rashid Mokhtar Al-Awadi. MRI brain tumor segmentation system based on hybrid clustering techniques. In the Second International Conference of Advanced Machine Learning Technologies and Applications -, AMLTA, pages 401–412, 2014.

[10] Jayram K. Udupa and K. Saha Punam. Fuzzy connectedness and image segmentation. Proceedings of the IEEE, 91:1649–1669, 2003.

[11] N. Menon, R. Ramakrishnan. Brain tumor segmentation in mri image using unsupervised artificial bee colony and fcm clustering. International Journal of Computer Science and Management Research, 2:2450–2454, 2013.

[12] Mutasem K. Alsmadi. Mri brain segmentation using a hybrid artificial bee colony algorithm with fuzzy-c mean algorithm. Journal of Applied Sciences, 15:100–109, 2015.

[13] D.M. Joshi, N. K. Rana, and V.M. Misra. Classification of brain cancer using artificial neural network. International Conference on Electronic Computer Technology (ICECT), pages 112–116, 2010.

[14] Sudipta Acharya, Yamini Thadisina, and Sriparna Saha. Multi-objective clustering of tissue samples for cancer diagnosis. International Conference on Advances in Computing, Communications and Informatics, pages 1059–1064, 2014.

[15] Anirban Mukhopadhyay, Ujjwal Maulik, and Sanghamitra Bandyopadhyay. Multiobjective genetic clustering with ensemble among pareto front solutions: Application to mri brain image segmentation. In Proceedings of the Seventh International Conference on Advances in Pattern Recognition, ICAPR '09, pages 236–239, 2009.

[16] Saha Sriparna and Bandyopadhyay Sanghamitra. Mri brain image segmentation by fuzzy symmetry based genetic clustering technique. In Proceedings of the IEEE Congress on Evolutionary Computation, CEC'2007, pages 4417–4424, 2007.

[17] Saha Sriparna and Bandyopadhyay Sanghamitra. Mr brain image segmentation using a multiseed based automatic clustering technique. Fundamenta Informaticae, 97(1):199–214, 2009.

[18] limam Olfa. Brain tumor segmentation using multiobjective fuzzy clustering. Transactions on Machine Learning and Artificial Intelligence, 4(1):58–67, 2016.

[19] Bong Chin-Wei and Mandava Rajeswari. Multiobjective optimization approaches in image segmentation - the directions and challenges. International Journal of Advances in Soft Computing and Its Applications, 2(2):41–64, 2010.

[20] Anil Kumar Jain, M Narasimha Murty, and Patrick Joseph Flynn. Data clustering: A review. ACM Computing Surveys, 31(3):265–323, 1999.

[21] Abhay Kumar Alok, Asif Ekbal, and Sriparna Saha. Brain image segmentation using semisupervised clustering. Expert Systems with Applications, 52:50–63, 2016.

[22] Brainweb: Simulated brain database, 2011, available at http://www.bic.mni.mcgill.ca/brainweb.

SOCIETY FOR SCIENCE AND EDUCATION UNITED KINGDOM

JBEMi JOURNAL OF BIOMEDICAL ENGINEERING AND MEDICAL IMAGING

ISSN: 2055-1266
VOLUME 3 ISSUE 2

Influence of BMI on Elastographic Strain Ratios of Achilles Tendon

Mahdi Al-Qahtani, Abdullah Al-Zahrani, AbdulAziz Al-Mujalli and Eraj Humayun Mirza
Department of Biomedical Technology, College of Applied Medical Sciences, King Saud University, Riyadh, KSA.
amahdi@ksu.edu.sa; abdfer4@gmail.com; aziiz.m.93@gmail.com; emirza@ksu.edu.sa

ABSTRACT

The Achilles tendon have two major problems due to injury; one being a chronic injury called Achilles tendinopathy and the second being acute injury which are more commonly known as Achilles tendon rupture. Changes in stiffness of Achilles tendon is alarming and can cause deleterious effects on quality of life in an individual. Achilles tendon is reported to be affected significantly due to the weight of an individual. The effect of Body Mass Index (BMI) on stiffness of Achilles tendon was evaluated in the current study. Elastography was performed on individuals ranging from 19 to 23 years for detecting the stiffness of the Achilles tendon. Individuals were grouped according to their BMI in 3 categories (underweight, normal and overweight) and their strain ratios were measured. The strain ratio results for all volunteers were ranging from 1.03 to 6 (1.03 for underweight and 6 for overweight). Difference in weight of individuals effect the Achilles tendon stiffness. The overweight individuals had the highest stiffness while the underweight individuals had the lowest. It is concluded that higher stiffness may likely lead to Achilles tendon injury.

Keywords: Elastography, Body Mass Index, Ultrasound, Achilles tendon, stiffness.

1 Introduction

The Achilles tendon joins two heads of the gastrocnemius muscle with soleus muscle. In the human body Achilles tendon is the strongest and the largest tendon. It bears forces up to 12.5 times of the actual weight of the body while sprinting [1]. Because the size of Achilles tendon and its demand it is injured easily [2].

Achilles tendon is a tough band tissue that connect the muscle with bone, it is the largest tendon in human body, it supports the activity of human body like walking, running and jumping [3].

Achilles tendon can get injured and the most common problem in Achilles tendon due to stiffness is Achilles tendinitis [4]. Overweight/ Obese people (high BMI, more then 25) are more prone to get Achilles tendonitis[5, 6].

Achilles tendinitis is Inflammation of the Achilles tendon [7]. During Achilles tendinitis the tendon tends to be stiffer than normal that decreases the movement and increases the pain [4].

DOI: 10.14738/jbemi.32.1957
Publication Date: 27th April 2016
URL: http://dx.doi.org/10.14738/jbemi. 32.1957

Achilles tendinitis occurs due to increase in physical activity, like walking extensively or running for a long time. Another reason for Achilles tendinosis is increased activity levels after a long periods or intervals of inactivity. Furthermore, weakness in the calf muscle is also related to Achilles tendinosis. Bearing significantly higher weight than normal also gives rise to Achilles tendinitis [8].

Prior to the use of ultrasound to determine stiffness in Achilles tendon, palpation was widely adopted. Palpation is the process of examining the features physically. However, this greatly depends upon the experience of the observer and it had various limitations like repeatability and reproducibility of the results. It's limited to accessible organ and not accurate.

Various studies have shown successful use of ultrasound for the detection of Achilles Tendinosis. However, ultrasound diagnosis for Achilles tendinosis has demonstrated some limitations in terms of determining the stiffness of the tendon.

Elastography is new technique that detects Achilles tendon; it's an enhanced form of ultrasound. It's better than palpation and ultrasound because it detect mechanical properties like stiffness/strain ratio. The Ultrasound Elastography has various types; most commonly used technique are Strain Elastography (SE) and Shear Wave Elasticity Imaging (SWEI) [9].

This study aims to determine the effect of Body Mass Index (BMI) on stiffness of Achilles tendon among young Saudi population. Furthermore, the objective of this study is to provide first-hand information to the clinicians on current health status of young Saudi population.

2 Materials and Methods

Fifteen healthy individuals were invited and divided into 3 groups with reference to BMI (underweight, normal weight and overweight).The BMI of each individual was calculated using formula stated in equation 1.

$$BMI = \frac{Weight}{Height^2} \tag{1}$$

- Where:
    a. Weight is in Kg
    b. height is in meters

All the volunteers were divided according to their BMI in 3 groups as mentioned earlier. All volunteers had sedentary life style. Average age for the volunteers was 21.8 years while they ranged from 19 to 23 years. Average weight for the volunteers was 74.5 Kg, while minimum weight was 42.8 Kg and maximum weight was recorded to be 140.9 Kg. Volunteers had an average height of 1.729m while their height varied from 1.64 to 1.84 m.

In order to determine the proximal and distal ends of the Achilles tendon, B-Mode ultrasound examination was performed at a gain of 50% and a frequency of 10 MHz with a linear probe (L14-5/38) on only right leg of individuals in prone position via SonixTouch Q+ from BK Ultrasound, Analogic Corporation, 8 Centennial Drive, Peabody, MA, USA. Throughout the examination the right leg of the individuals was left hanging from the distal edge of the examination couch as shown in figure 1.

Figure 1. Examination of central part of Achilles tendon as marked by the box. The green line shows the length of Achilles tendon determined via B-mode ultrasound.

After determining the length of Achilles tendon a marker was used to mark the length of Achilles tendon and calculate the central region. Elastography was performed in the central region only with linear probe in longitudinal direction.

From a cine loop of 99 images, 5 best images were selected that were in range of strain sensor. Out of the 5 images selected, 3 random region of interest (ROI) were selected from Achilles tendon and surrounding tissue respectively to determine the strain ratios.

The current study was conducted at department of biomedical technology, college of applied medical sciences, King Saud University. All the examination was performed at room temperature. Previously described protocol for Achilles tendon ultrasound was used [10] and all parameters of the ultrasound elastography machine were kept constant throughout the study.

2.1 Elastographic Strain ratio

After examining the B-mode image, elastographic mode was selected to measure the strain ratios of the tumor. To determine strain ratios at 3 different locations; one area within the tumor while other area outside the tumor but within the thyroid gland was selected as shown in figure 2.

COPYRIGHT© SOCIETY FOR SCIENCE AND EDUCATION UNITED KINGDOM

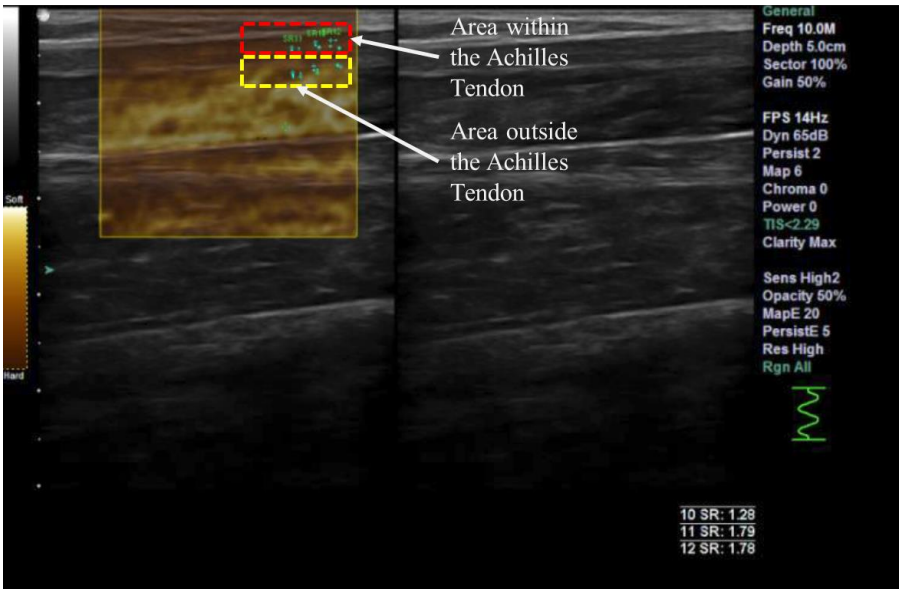

Figure 2. Elastographic and B-mode image for Achilles tendon. Red and Yellow dashed box indicated random location selected to determine strain ratio.

3 Results

The BMI results of the underweight volunteers were observed to be from 15.53 to 18.36, with an average BMI of 17.18 ± 1.21. Volunteers with normal BMI initiated with a BMI of 18.96 until 23.88, while the average recorded was 21.232 ± 1.74. Overweight volunteers demonstrated highest BMI ranging from 26.65 to 44.47, while their average was 35.836 with standard deviation of 7.68.

Length of Achilles tendon did not played any role in the stiffness as it can be observed from table 4.1. No significant difference was observed among the length of Achilles tendon between the groups.

Table 1. Length of Achilles tendon among different groups

Length	Lowest Reading	Highest Reading	Average ± STD DEV
Underweight	21	25	**22.5**
Normal weight	21	24	**22.1**
Overweight	20.5	26	**22.7**

The Strain Ratio results (figure 1) of the Underweight Volunteers demonstrated lowest values among all the group ranging from 1.03 to 2.52, with an Average of 1.627 having standard Deviation of 0.069. Normal weight volunteers had strain ratios of 1.65 to 4.12, with average of 2.617 and a standard deviation of 0.133. Moreover, overweight volunteers had the highest strain ratios, with a minimum of 2.31 while going up to 6, the average strain ratio in this category was recorded to be 4.294 with a standard deviation of 1.125. Significant differences can be observed between all the groups.

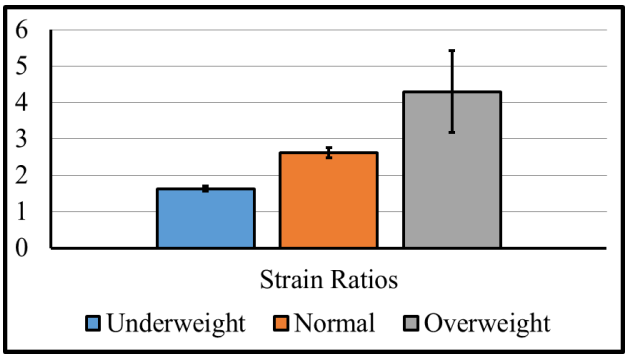

Figure 3 Strain ratios of Achilles tendon among different groups.

Elastographic images for different BMI group demonstrates that in case of underweight volunteer the Achilles tendon have bright color and the strain ratio have a low reading that's mean Achilles tendon not very stiff.

As shown in Figure 3, the Achilles tendon surrounding by muscle and skin, the Achilles tendon has unidirectional muscle fibers, while surrounding muscle has randomly arranged fibers.

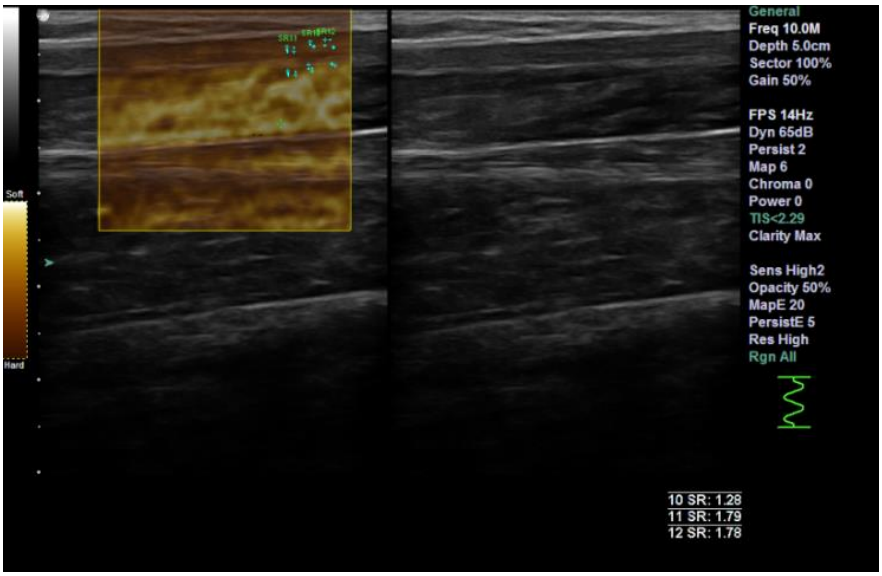

Figure 4 Elastographic and B-mode image for Achilles tendon of underweight individual.

Figure 4 shows Achilles tendon of volunteers having normal weight. It was observed that B-mode ultrasound image for Achilles tendon is not very bright color and the strain ratio have a normal reading that's mean Achilles tendon stiffer when compared to their underweight counterparts.

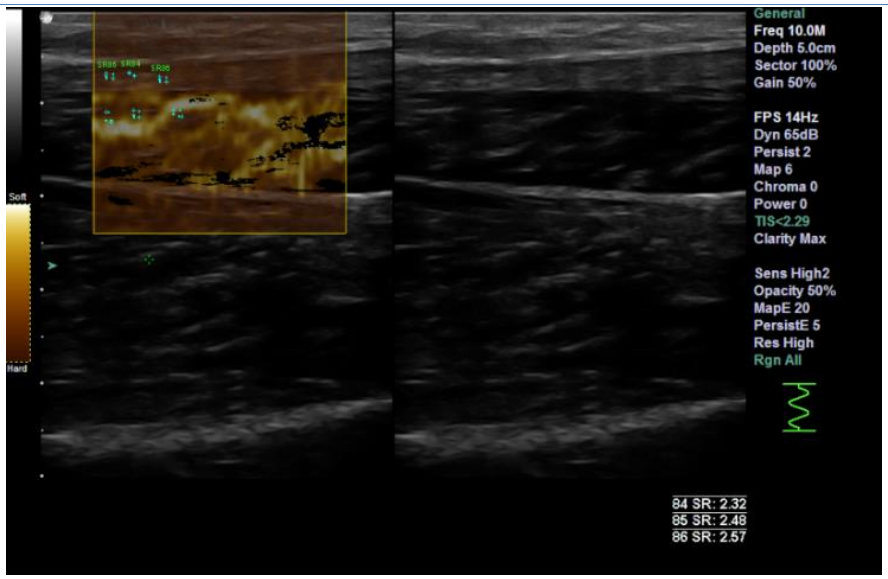

Figure 5 Elastographic and B-mode image for Achilles tendon of normal weight individual.

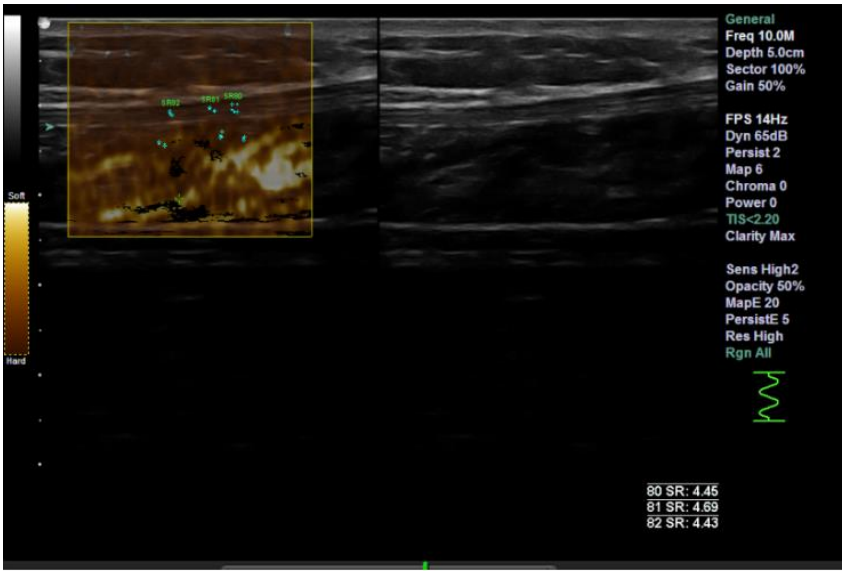

Figure 6 Elastographic and B-mode image for Achilles tendon of overweight individual.

For overweight volunteer B-mode image in figure 6 displays the Achilles tendon to have very dark grey scale and the strain ratio have a high reading meaning that stiffness of Achilles tendon is significantly different than its surrounding tissue.

4 Discussion

It was observed that strain ratios were directly proportional to the BMI of an individual, irrespective of their Achilles tendon length.

Other researchers have reported that elastography compares well with ultrasound for Achilles tendon. They found that Achilles tendon among normal individuals is hard when compared to surrounding

tissues [11]. Similar results were observed in our study, where all the volunteers demonstrated their Achilles tendon to be stiffer than surrounding tissue irrespective of their BMI.

Elastographic images for different BMI groups demonstrated a clear visual difference among the Achilles tendon. The Achilles tendon for underweight individuals was much clear when compared to normal and overweigh individuals. Furthermore, it was observed through the elastographic images that the individuals that fall in the category of overweight had a significantly higher amount of fat deposition around the Achilles tendon.

Moreover, Elastographic pattern for images with respect to BMI demonstrated that higher the BMI the greater is the tissue stiffness variation between Achilles tendon and surrounding tissue.

5 Conclusion

It was concluded that difference in weight (refer to BMI) effect the Achilles tendon stiffness, the overweight people (refer to BMI) they have highest stiffness, when compared to the normal weight and for underweight people. The stiffness in Achilles is likely to increase the possibility of Achilles tendon injury. Young people must be advised to perform regular exercise to maintain a balance in their BMI. Moreover, further studies are required to ascertain the findings.

Current study only comprise of male volunteers who had sedentary activity throughout the day. Results presented in this report are for an age group of 19 to 23.

It is recommended that future studies must also be carried on females and on a larger population with diverse ages. Secondly, strain ratios must be obtained at different settings of the ultrasound machine to make sure the repeatability of results. We suggest that in future the research should be directed towards comparison of strain elastography with other types of elastography techniques in order to ascertain the repeatability of results from different techniques.

ACKNOWLEDGEMENT

The authors would like to extend their appreciation to the College of Applied Medical Sciences Research Center and the Deanship of Scientific Research at King Saud University for funding this research.

REFERENCES

[1]. Paavola, M., et al., *Achilles tendinopathy.* The Journal of Bone & Joint Surgery, 2002. 84(11): p. 2062-2076.

[2]. Nickisch, F., *Anatomy of the Achilles tendon*, in *The Achilles Tendon*. 2009, Springer. p. 2-16.

[3]. Fletcher, J.R., et al., *Achilles tendon strain energy in distance running: consider the muscle energy cost.* Journal of Applied Physiology, 2015. 118(2): p. 193-199.

[4]. Kubo, K., et al., *Relationship between elastic properties of tendon structures and performance in long distance runners.* European journal of applied physiology, 2015: p. 1-9.

[5]. Franceschi, F., et al., *Obesity as a Risk Factor for Tendinopathy: A Systematic Review.* International Journal of Endocrinology, 2014. 2014: p. 10.

[6]. Klein, E.E., et al., *Body mass index and achilles tendonitis: a 10-year retrospective analysis.* Foot Ankle Spec, 2013. 6(4): p. 276-82.

[7]. Vieira, C.P., et al., *Glycine improves biochemical and biomechanical properties following inflammation of the Achilles tendon.* The Anatomical Record, 2015. 298(3): p. 538-545.

[8]. Alfredson, H., et al., *Heavy-load eccentric calf muscle training for the treatment of chronic Achilles tendinosis.* The American Journal of Sports Medicine, 1998. 26(3): p. 360-366.

[9]. Al-Qahtani, M., et al., *A Comparative Study of Shear-Wave Elastography and Strain Elastography on a Breast Phantom for Diagnosis of Tumor and Cyst.* 2015, 2015. 2(3).

[10]. Radiology, A.C.o., *AIUM practice guideline for the performance of a musculoskeletal ultrasound examination.* Journal of ultrasound in medicine: official journal of the American Institute of Ultrasound in Medicine, 2012. 31(9): p. 1473.

[11]. De Zordo, T., et al., *Real-time sonoelastography findings in healthy Achilles tendons.* American Journal of Roentgenology, 2009. 193(2): p. W134-W138.

THE END

Multiple Hand Gesture Recognition using Surface EMG Signals

Nazo Haroon[1]and Anjum Naeem Malik[2]
National University of Sciences & Technology, Islamabad, Pakistan.
[1]nazoharoon78@mts.ceme.edu.pk; [2]anjum.naeem78@mts.ceme.edu.pk

COPYRIGHT© SOCIETY FOR SCIENCE AND EDUCATION UNITED KINGDOM

ABSTRACT

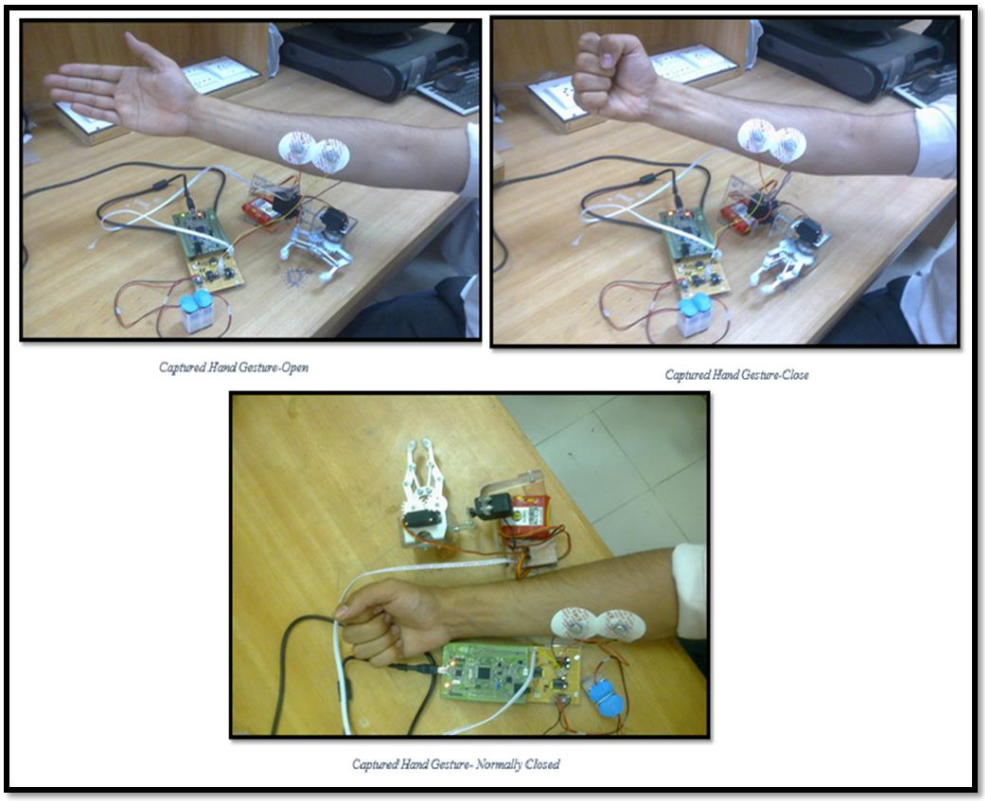

Figure 9. Results of different gestures detected

6 Conclusion

Electromyographic signal contains valuable information regarding the nervous system so the main objective of this study was to give a brief information about EMG signals acquisition, analysis and interfacing methodologies with exoskeleton/robotic gripper. This study clearly differentiated gestures of upper limb (open, close, normally close and wrist downward movement) and interfaced successfully with the robotic gripper using STM32F40xx discovery board controller. While implementing the hardware interface it has been observed that use of other reconfigurable devices like FPGA and PLDs will enhance the results in more efficient way. Future work will comprise of enhancing signal processing techniques and lower limb prosthetics interfacing with SEMG electrodes.

REFERENCES

[1] Shahid S. Higher Order Statistics Techniques Applied to EMG Signal Analysis and Characterization. Ph.D. thesis, University of Limerick; Ireland, 2004.

[2] Nikias CL, Raghuveer MR. Bispectrum estimation: A digital signal processing framework. IEEE Proceedings on Communications and Radar. 1987; 75 (7):869–891.

[3] Basmajian JV, de Luca CJ. Muscles Alive - The Functions Revealed by Electromyography. The Williams & Wilkins Company; Baltimore, 1985.

[4] Cram JR, Kasman GS, Holtz J. Introduction to Surface Electromyography. Aspen Publishers Inc.; Gaithersburg, Maryland, 1998.

[5] Thexton AJ. A randomization method for discriminating between signal and noise in recordings of rhythmic electromyographic activity. J Neurosci Meth. 1996; 66: 93 –98.

[6] Bornato P, de Alessio T, Knaflitz M. A statistical method for the measurement of the muscle activation intervals from surface myoelectric signal gait. IEEE Trans Biomed Eng.1998; 45: 287–299. doi: 10.1109/10.661154.

[7] Merlo A, Farina D. A Fast and Reliable Technique for Muscle Activity Detection from Surface EMG Signals. IEEE Trans Biomed Eng. 2003; 50 (3):316–323. Doi: 10.1109/TBME.2003.808829.

[8] Gabor D. Theory of communication. J Inst Elect Eng.1946; 93:429–457.

[9] Hefftner G, Zucchini W, Jaros G. The electromyogram (EMG) as a control signal for functional neuro-muscular stimulation part 1: Autoregressive modeling as a means of EMG signature discrimination. IEEE Trans Biomed Eng.1988; 35:230–237. doi: 10.1109/10.1370.

[10] Christodoulou CI, Pattichis CS. A new technique for the classification and decomposition of EMG signals. Proceedings in IEEE International Conference on Neural Networks.1995; 5:2303–2308.

[11] H. Arieta, R. Katoh, H. Yokoi, Y. Wenwei, 2006Development of a multi-DOF electromyography prosthetic system using the adaptive joint mechanism, ABBI 2006, 32110.

COPYRIGHT© SOCIETY FOR SCIENCE AND EDUCATION UNITED KINGDOM

SOCIETY FOR SCIENCE AND EDUCATION
UNITED KINGDOM

JBEMi JOURNAL OF BIOMEDICAL ENGINEERING AND MEDICAL IMAGING

ISSN: 2055-1266
VOLUME 3 ISSUE 2

DOI: 10.14738/jbemi.31.1892
Publication Date: 27th February 2016
URL: http://dx.doi.org/10.14738/jbemi. 31.1892

SOCIETY FOR SCIENCE AND EDUCATION
UNITED KINGDOM

JBEMi JOURNAL OF BIOMEDICAL ENGINEERING AND MEDICAL IMAGING

ISSN: 2055-1266
VOLUME 3 ISSUE 2

DOI: 10.14738/jbemi.26.1732
Publication Date: 29th December 2015
URL: http://dx.doi.org/10.14738/jbemi. 26.1732